Nucleobases Undergo Dynamic Rearrangements during RNA Tertiary Folding

Robb Welty and Kathleen B. Hall

Department of Biochemistry and Molecular Biophysics, *Washington University School of Medicine, St. Louis, MO 63110, USA*

Correspondence to Kathleen B. Hall: *kathleenhal@gmail.com*
http://dx.doi.org/10.1016/j.jmb.2016.09.015
Edited by Sarah A. Woodson

Abstract

The tertiary structure of the GTPase center (GAC) of 23S ribosomal RNA (rRNA) as seen in cocrystals is extremely compact. It is stabilized by long-range hydrogen bonds and nucleobase stacking and by a triloop that forms within its three-way junction. Its folding pathway from secondary structure to tertiary structure has not been previously observed, but it was shown to require Mg^{2+} ions in equilibrium experiments. The fluorescent nucleotide 2-aminopurine was substituted at selected sites within the 60-nt GAC. Fluorescence intensity changes upon addition of $MgCl_2$ were monitored over a time-course from 1 ms to 100 s as the RNA folds. The folding pathway is revealed here to be hierarchical through several intermediates. Observation of the nucleobases during folding provides a new perspective on the process and the pathway, revealing the dynamics of nucleobase conformational exchange during the folding transitions.

Introduction

RNA tertiary structures can often be visualized as interactions between discrete structural elements, but de novo prediction of those interactions is often impossible. Uncertainty and ambiguity arise from the number of potential interactions between known elements (such as a tetraloop/tetraloop receptor) and between elements that have unrecognized contributions (such as loops). Tertiary interactions, such as hydrogen bonding, stacking, and ion chelation, can be identified in RNA crystal structures and then modeled into novel RNA sequences. More examples of interactions are necessary to develop a tool box for modeling, but equally necessary is the knowledge of how different interactions are temporally ordered during the formation of a functional RNA tertiary structure.

The 60-nt GTPase center (GAC) of 23S/28S ribosomal RNA is seen in cocrystals and X-ray and cryo-electron microscopy structures of the ribosome to adopt an intricate tertiary fold. GAC secondary structure is highly conserved among kingdoms [1]. Its tertiary structure is known from two GAC cocrystals with L11 protein [2,3] and several ribosome structures [4–6]. Cocrystals show multiple base triples that anchor distal secondary structures, U-turns, a triloop, long-range nucleobase stacking, long-range hydrogen bonding, and chelated ions. The GAC facilitates ribosome function through its interactions with EF-G and the L11 protein, which occur when the GAC is folded. The folding process, from secondary structure to tertiary structure, is unknown.

RNA tertiary folding requires charge neutralization of the phosphodiester backbone to allow the close approach of phosphates in a packed RNA. Many RNAs use divalent ions to efficiently shield proximal phosphates, and *in vivo*, Mg^{2+} ions are the most abundant. Mg^{2+} ions appear in virtually all X-ray crystal structures of RNAs, although while in solution, most Mg^{2+} ions appear diffusely associated with RNA molecules. In physiological solutions with monovalent ions, Mg^{2+} will neutralize phosphate charges more efficiently and hence will be preferentially associated with an RNA strand. It is difficult to assign specific contributions of Mg^{2+} ions to the process of RNA tertiary folding.

Structure/function studies of *Escherichia coli* GAC identified a single nucleotide substitution that conferred a requirement for Mg^{2+} ions to adopt its tertiary fold [7]. Of the 58 GAC nucleobases, 12 are completely conserved throughout all kingdoms (Fig. 1),

Please cite this article as: R. Welty, K. B. Hall, Nucleobases Undergo Dynamic Rearrangements during RNA Tertiary Folding, J. Mol. Biol. (2016), http://dx.doi.org/10.1016/j.jmb.2016.09.015

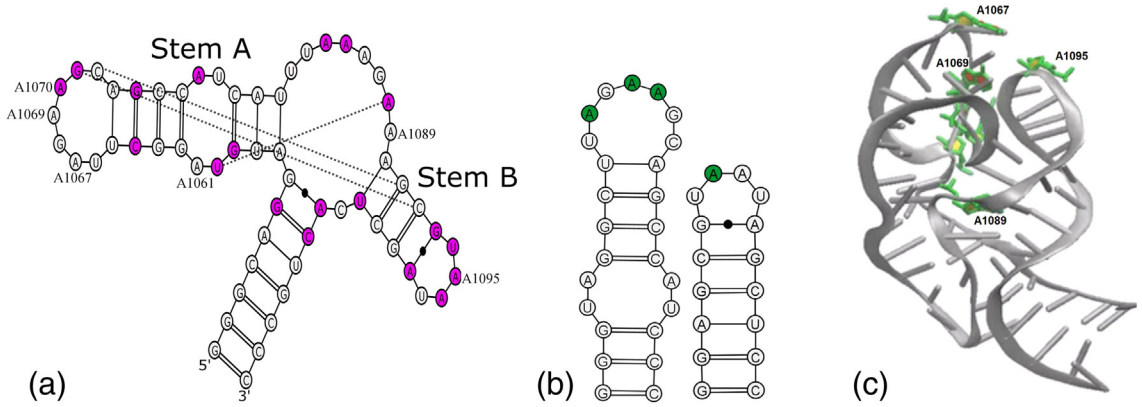

Fig. 1. (a) Secondary structure of the *E. coli* GAC U1061A, with phylogenetically conserved bases in magenta and tertiary contacts observed in the cocrystals indicated by lines. Numbered nucleotides were substituted with 2AP. (b) Sequences of hairpin constructs with sites of 2AP substitution in green. (c) Cocrystal structure (1HC8) of *E. coli* GAC with 2AP substitution sites in green.

but those sites that vary (and co-vary) allow substitutions to be introduced and tested for structure/function. In particular, position 1061 is 58% uridine, 36% guanine, and 6% adenine [8]. Curiously, the distribution largely follows phylogenetic classifications: uridine is found in eubacteria, guanine in eukaryotes, and some archaebacteria have adenine. Substituting the natural *E. coli* U1061 with A1061 (Fig. 1) produced a GAC that was active *in vivo* [9], but *in vitro*, it would not adopt a tertiary structure in the absence of Mg^{2+} ions. Thermodynamic characterization of this *E. coli* U1061A variant [2,10,11] led to the conclusion that a single Mg^{2+} ion could make a large contribution to its folding free energy [12]. Combining thermodynamic data with cocrystal structures of the GAC with L11, Leipply and Draper identified a specific chelated Mg^{2+} ion as responsible for the stabilization of the tertiary structure [12]. In the cocrystal structure (pdb 1hc8 [2]), the phosphate of nucleotide A1073 appears to chelate both a K^+ ion and this specific Mg^{2+} ion, holding them both in an electronegative pocket. This pocket is formed by tertiary interactions that stabilize the juxtaposition of the two hairpins. Does the Mg^{2+} ion trap a conformation of the GAC, stabilizing it to anchor the tertiary fold (conformational selection)? Does the Mg^{2+} ion alter the structure of the GAC to create its own binding pocket (induced fit [13])? Equilibrium methods and crystal structures cannot distinguish between these alternatives, but a kinetic study of GAC folding might provide some insight.

RNA tertiary folding has been characterized for several RNA molecules. RNA folding can be initiated by the introduction of specific ions (typically Mg^{2+}), then the temporal progress of chemical probing of the phosphodiester backbone is monitored in quenched-flow experiments. Time scales and intermediates during tertiary structure formation have been identified for the 414-nt *Tetrahymena* group I intron [14–20] and the 215-nt *Azoarcus* group I intron [21–24]. Folding of the *Tetrahymena* group I intron has been mapped by time-resolved hydroxyl radical footprinting, revealing a hierarchical folding pathway [25,26]. The time scales of steps in its folding range from milliseconds to tens of seconds; several intermediates have been identified and misfolding has been consistently observed [17,27–29]. Folding pathways of the *Azoarcus* group I intron have also been probed by time-resolved hydroxyl radical footprinting and 2-aminopurine (2AP) fluorescence [21]. These have been powerful methods for mapping the folding process of group I introns and their substructures.

For the GAC, we wanted to observe the nucleobases directly in order to monitor how and when they formed their interactions that created and stabilized the tertiary fold. Here, we took advantage of known properties of the GAC. The *E. coli* U1061A:*Bacillus stearothermophilus* L11 cocrystal (pdb 1hc8) allowed us to identify those nucleobases that stacked with other nucleobases but did not make hydrogen bonds. With this information, we substituted 6 nt with the fluorescent nucleobase 2AP, which should not alter the tertiary structure of the GAC as we predicted. Mg^{2+}-dependent tertiary folding of these six RNAs was studied by stopped-flow fluorescence, allowing the observation of fluorescence intensity on time scales from millisecond to second. We find multiple states along a folding pathway that includes several Mg^{2+}-dependent intermediates. Most strikingly, we observe dynamic conformational exchanges of nucleobases from stacked →unstacked →stacked as the GAC folds. From our time-resolved and steady-state fluorescence data, we constructed a model of how the GAC folds that incorporates its Mg^{2+} dependence and its conformational changes.

Please cite this article as: R. Welty, K. B. Hall, Nucleobases Undergo Dynamic Rearrangements during RNA Tertiary Folding, J. Mol. Biol. (2016), http://dx.doi.org/10.1016/j.jmb.2016.09.015

Results

The sequence of the *E. coli* GAC with the U1061A substitution is given in Fig. 1. Six GAC RNAs constructs were chemically synthesized [30] by Agilent Labs, each with a single 2AP substitution. Three substitutions were placed in the 5′ hairpin loop (A1067AP, A1069AP, and A1070AP) which, as shown in the cocrystal [2], arranges the first five bases (U1065 to A1069) in a U-turn conformation and extrudes the 3′ three bases (A1070/G1071/C1072) to create what we refer to here as a T+loop [31,32]. The A1089AP substitution was designed to monitor the three-way junction. The A1061AP substitution probes the internal bulge in the 5′ hairpin stem. The A1095AP substitution monitors the 3′ hairpin loop (U1092/A1079), which is a canonical U-turn [33].

2AP substitution does not alter GAC tertiary structure formation

The six 2AP-GAC constructs were compared to *in vitro* transcribed GAC to measure the thermal stability of their secondary structure, tertiary structure, and response to Mg^{2+}. Thermal denaturation, monitoring the absorbance at 260 nm and 280 nm, was previously shown to report the stability of GAC secondary and tertiary structures [7,12]. Transition temperatures of the 2AP-GAC were nearly identical to the unmodified GAC (Fig. 2). Based on those criteria, we conclude that each 2AP-GAC construct adopted the predicted secondary structure and required Mg^{2+} to form a tertiary structure.

As another measure of structure formation, we used time-resolved fluorescence anisotropy [34] to observe the global rotational correlation time of 2AP-GAC molecules. Depolarization of 2AP in the RNAs is dependent on the global rotation of the molecule and on local motions. We predicted that these values in the secondary and tertiary structure would be different.

Measured fluorescence anisotropy decay curves for each 2AP site were fit by one or two exponential components. We globally fit the longest rotational correlation time of the data from every 2AP construct by $\varphi 1 = 6.5 \pm 0.08$ ns in the absence of Mg^{2+} and by $\varphi 1 = 7.5 \pm 0.05$ ns in the presence of 8 mM Mg^{2+}. The goodness of fit of all sites to these values suggests that each site is reporting on a common global structure. While we anticipated that a compact tertiary fold should result in such agreement, it is rather surprising that the secondary structure values are so consistent. We can account for the result if the GAC arms have relative motion in the secondary structure, which would result in a shorter depolarization time.

2AP sites report on the GAC tertiary fold

Each 2AP site exhibits a unique fluorescence response to the addition of Mg^{2+} that reflects its environment. We interpret fluorescence intensity in terms of base stacking: low intensity is consistent with quenching by nucleobase stacking, and high intensity corresponds to a more unstacked 2AP [35]. Time-resolved fluorescence lifetimes report on conformational states accessible to 2AP, and time-resolved anisotropy reports on global and local motions. We observe multi-exponential fluorescence lifetimes for 2AP in all sites in the GAC, and most sites also have an anisotropy (depolarization) component consistent with local motion (Supplementary Table 1). These data show that no 2AP nucleobase is rigidly fixed; 2AP in all six sites undergoes picosecond–nanosecond local conformational sampling.

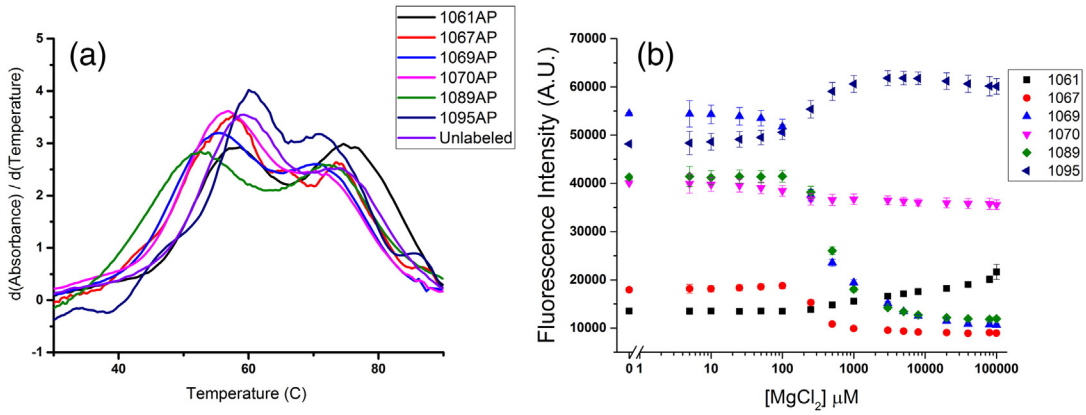

Fig. 2. Mg^{2+} dependence of 2AP-GAC stability. (a) First derivative of absorbance (A_{260}) *versus* temperature (dA/dT), which reveals the conformational transitions of the RNAs. Melting was measured in 100 mM KCl, 3 mM $MgCl_2$, and 10 mM sodium cacodylate (pH 6.5). The lower temperature transition is assigned to tertiary structure melting; the second transition is secondary structure melting. (b) $MgCl_2$ titration of 2AP fluorescence at 20 °C; [GAC] = 2 µM in 100 mM KCl and 10 mM sodium cacodylate (pH 6.5).

Please cite this article as: R. Welty, K. B. Hall, Nucleobases Undergo Dynamic Rearrangements during RNA Tertiary Folding, J. Mol. Biol. (2016), http://dx.doi.org/10.1016/j.jmb.2016.09.015

The Mg^{2+} concentration dependence of each 2AP-GAC was measured using steady-state fluorescence. GAC secondary structure was formed prior to $MgCl_2$ titration (Materials and Methods). The relative change in fluorescence intensity, for 1 μM GAC, was site specific, as shown in Fig. 2. Each construct showed an approximate midpoint of transition from 0.3 to 0.5 mM $MgCl_2$ and reaches a plateau by 3 mM $MgCl_2$. We conclude that 3 mM Mg^{2+} is saturating.

Steady-state 2AP fluorescence intensity varies by site. In Mg^{2+} titrations, A1061AP fluorescence intensity is consistently low, indicating that it is mostly stacked with or without Mg^{2+}. A1095AP at the apex of a U-turn shows an increase in fluorescence intensity with added Mg^{2+}. A1089AP in the three-way junction loses about a third of its fluorescence intensity in the presence of Mg^{2+}. T+loop A1067AP fluorescence intensity is uniformly low, suggesting that it is mostly stacked. In contrast, A1070AP fluorescence is high, regardless of Mg^{2+} concentration, consistent with unstable stacking. A1069 fluorescence has a substantial intensity difference before and after Mg^{2+} addition. Together, these data suggest that the T+loop and the junction undergo a conformational change.

The local thermal stability at each 2AP site was compared by fluorescence to the thermal stability of the entire tertiary structure, which was measured by UV absorbance. In the presence of Mg^{2+}, the melting transitions for the tertiary and secondary structures occur at 56–60 °C and 75 °C, respectively, whereas in the absence of Mg^{2+}, a single broad transition occurs at 43–60 °C [36]. Fluorescence intensity of each 2AP-GAC was measured during thermal denaturation in the presence and absence of 3 mM $MgCl_2$ (Supplementary Fig. 1). Secondary structure denaturation in the absence of Mg^{2+} was only apparent in the 1061AP trace, presumably reporting on melting of the hairpin stem at the internal bulge. In contrast, tertiary structure melting in the presence of Mg^{2+} was observed for all sites with the exception of GAC-A1095AP, which is at the apex of the U-turn in stemloop B. At higher temperatures, progressive loss of fluorescence is attributed to collisional quenching [34] with solvent or adjacent nucleotides as the RNA structure is disrupted.

Stopped-flow fluorescence data reveal multiple intermediate folded states

Steady-state experiments showed that each 2AP site was sensitive to environmental changes upon tertiary structure formation. Now, we ask how fluorescence intensity changes during the folding process. For these experiments, we use stopped-flow spectroscopy to rapidly mix the GAC with increasing amounts of $MgCl_2$ to observe the tertiary folding process in real time. All stopped-flow time-course traces (progress curves) are fit to a sum of exponentials to determine the relaxation times that define the kinetics of GAC folding [Eq. (1)].

GAC absorbance at 260 nm decreases upon tertiary structure formation. In stopped-flow absorbance experiments, we observed a trace that was fit by two

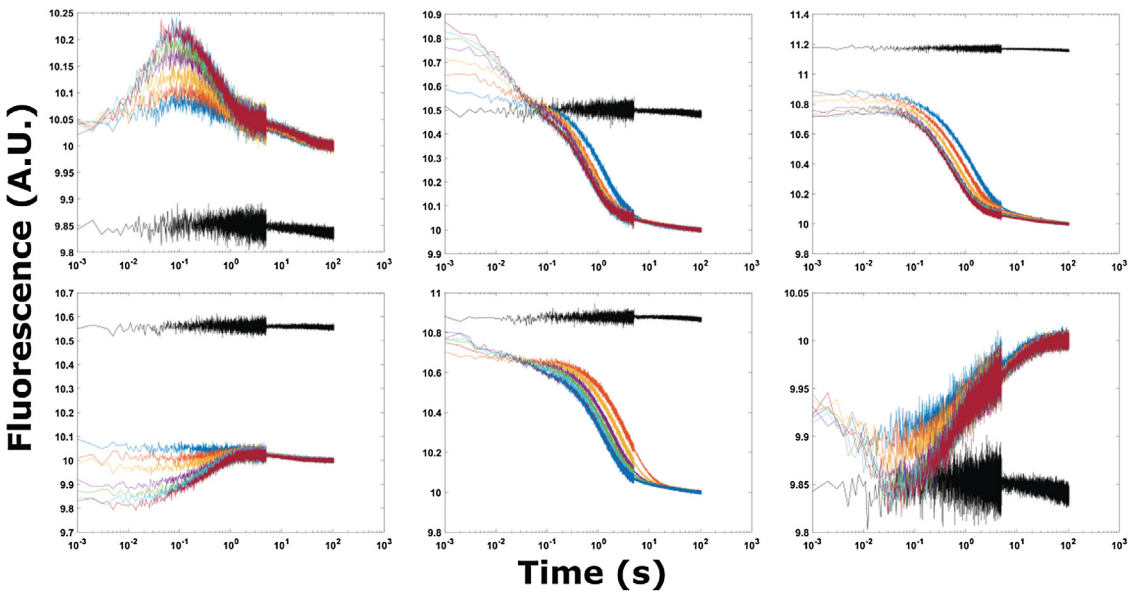

Fig. 3. Stopped-flow fluorescence traces of 2AP-GAC at 20 °C. Top row from left to right: A1061AP, A1067AP, A1069AP. Bottom row from left to right: A1070AP, A1089AP, A1095AP. $MgCl_2$ additions from 3 (blue), 5, 8, 20, 40, 80 to 100 (red) mM in 100 mM KCl, 10 mM sodium cacodylate. The black trace is buffer-only mixing control.

Please cite this article as: R. Welty, K. B. Hall, Nucleobases Undergo Dynamic Rearrangements during RNA Tertiary Folding, J. Mol. Biol. (2016), http://dx.doi.org/10.1016/j.jmb.2016.09.015

exponentials [36]. The dominant transition at 20 °C in 20 mM $MgCl_2$ had a time constant of ~660 ms, which we assign to tertiary folding.

In contrast to the traces from stopped-flow absorbance, stopped-flow fluorescence traces show transitions on four separate time scales. Each 2AP site on the GAC had a unique progress curve, with transitions ranging from less than a millisecond to the order of tens of seconds. Each trace was fit by three exponentials [Eq. (1)], giving three time constants (τ_1, τ_2, τ_3) that varied with the amount of Mg^{2+} added until the system was saturated (Fig. 4). Global analysis of five constructs at a given $MgCl_2$ concentration simultaneously fits the progress curves to Eq. (1), using the same values of the relaxation time parameters (τ_1, τ_2, τ_3) for all curves (Fig. 4).

$$y = y_0 + A_1 e^{\frac{-t}{\tau_1}} + A_2 e^{\frac{-t}{\tau_2}} + A_3 e^{\frac{-t}{\tau_3}} \quad (1)$$

where y is the fluorescence signal, y_o is an offset, A_n is the amplitude of the fluorescence signal change transition, and τ_n is the relaxation time of the fluorescence change.

The progress curves of five 2AP-GAC molecules were fit by identical relaxation times, suggesting that each RNA followed the same folding pathway (Table 1; A1089AP is an outlier). To generalize the results, we interpret our data using the framework of classical chemical kinetics to infer the lower limit of states in the folding pathway as one plus the number of observed transitions [37]. By this criterion, we have at least four transition states in the pathway.

The progress curves are fit by three quantifiable transitions that occur from tens of milliseconds (τ_1) to seconds (τ_2, τ_3). The shortest relaxation time increases at higher Mg^{2+} concentrations (in other words, the associated conformational transition is apparently slowed by the addition of Mg^{2+}). Because this transition occurs after the initial RNA/Mg^{2+} interaction (<1.5 ms; see below), it suggests that the GAC must undergo a conformational change [38] to a new Mg^{2+}-binding-competent state. These data support the hypothesis of Leipply and Draper [12] that the GAC has two distinct Mg^{2+} interactions. In contrast, the subsequent relaxation times, on the order of single and tens of seconds, become shorter with increasing Mg^{2+} concentrations until they reach a plateau (Fig. 4), perhaps reflecting a general shielding of phosphate charges.

A1089AP-GAC was the outlier in the global fits, so its kinetic data were fit independently to Eq. (1). Interestingly, the only prominent difference among the RNAs was the value of τ_2 of A1089AP-GAC (Table 1). On average, it is 55% longer than the analogous relaxation time of the other molecules. We speculate that it represents an additional intermediate state of the hinge region, possibly the formation of the triloop.

Taken together, we propose that the folding pathway of the GAC RNA consists of at least six resolvable species.

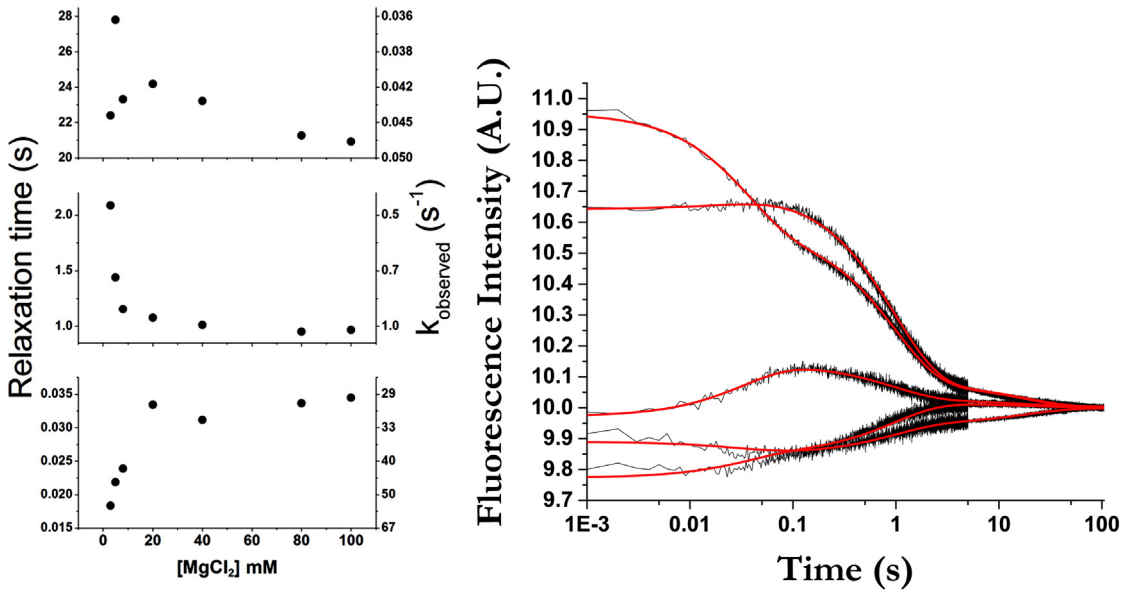

Fig. 4. Relaxation times and corresponding observed rates (1/τ) from global fits. Errors are contained within the data points. The scatter in the first points in the top plot is due to sparse sampling. An example of global fitting of stopped-flow traces for all 2AP-GAC molecules is shown for the addition of 20 mM $MgCl_2$. Black traces are data; red lines are fit. All progress curves and fits are shown in Supplementary Figs. 2 and 3.

Please cite this article as: R. Welty, K. B. Hall, Nucleobases Undergo Dynamic Rearrangements during RNA Tertiary Folding, J. Mol. Biol. (2016), http://dx.doi.org/10.1016/j.jmb.2016.09.015

Table 1. Relaxation times for 2AP-GAC folding transitions

	τ_1 (seconds)		τ_2 (seconds)		τ_3 (seconds)	
Construct	Global	1089AP	Global	1089AP	Global	1089AP
3 mM Mg^{2+}	0.018	–	2.1	3.8	22	26
5 mM Mg^{2+}	0.022	–	1.4	2.7	28	28
8 mM Mg^{2+}	0.024	0.007	1.2	2.0	23	25
20 mM Mg^{2+}	0.033	0.011	1.1	1.7	24	22
40 mM Mg^{2+}	0.031	0.014	1.0	1.4	23	20
80 mM Mg^{2+}	0.034	0.024	0.95	1.4	21	21
100 mM Mg^{2+}	0.034	0.027	0.97	1.3	21	21

Relaxation times calculated from global fitting and independent A1089AP curve fitting. The error generated by Origin software from the curve fit is uniformly <5% of the parameter value. 20 °C in 100 mM KCl and 10 mM sodium cacodylate (pH 6.5).

Isolating the source of rapid signal change

In addition to the measured transitions states, a first transition occurs during the dead time of our instrument (~1.5 ms) and is not represented in Eq. (1). The amplitude of this early transition is Mg^{2+}-dependent and varies with Mg^{2+} concentration; fluorescence intensity can either increase or decrease with respect to the starting value (Fig. 3). We conclude that the GAC undergoes a Mg^{2+}-dependent conformational transition during the rapid mixing process and before fluorescence is measured. This transition is visible in time-courses from all molecules and achieves an equilibrium before the recording of the fluorescence signal.

The source and nature of rapid conformational changes (<1 ms) from the association of divalent cations with RNA have been previously observed and attributed to electrostatic relaxation or counterion collapse [20,39–42]. This phenomenon is often associated with a rapid decrease in the radius of gyration of an RNA molecule, indicating a physical collapse. Indeed, previous small angle X-ray scattering (SAXS) experiments with the GAC have shown that it does undergo a physical compaction, from R_G = 25 Å to R_G = 15.9 Å, in the presence of Mg^{2+} [10]. The rapid signal change that occurs during our instrument's dead time could report on a global collapse of the GAC or, alternatively, could be caused by local conformational changes at each probed site in the GAC.

To differentiate the global *versus* local origins of this fast relaxation process, we compared the GAC properties to those of its two hairpins alone. Each hairpin was synthesized with a single 2AP to correspond to a position in the full GAC (Fig. 1b). The fluorescence intensity of A1067AP and A1070AP in the hairpin alone are consistent with unstacked nucleobases (Supplementary Fig. 4), whereas in the GAC, these sites are stacked. With this conformational difference in mind, the hairpin RNAs were also examined with stopped-flow fluorescence.

All four hairpin constructs exhibit a rapid change of fluorescence intensity within the dead time of the instrument but undergo no further transitions. Stopped-flow fluorescence of the 3′ hairpin with A1095AP illustrates these data (Fig. 5). Conformational changes within the RNA loops have been measured by several methods and have been shown to occur on the order of microseconds [43,44]. The relative increase or decrease of the hairpin fluorescence intensity corresponds to the analogous GAC construct, and we assign those signals to a local loop conformational change. However, the relative amplitudes of the signal change in hairpins and GAC are different, suggesting additional contributions from other events or interactions in the GAC.

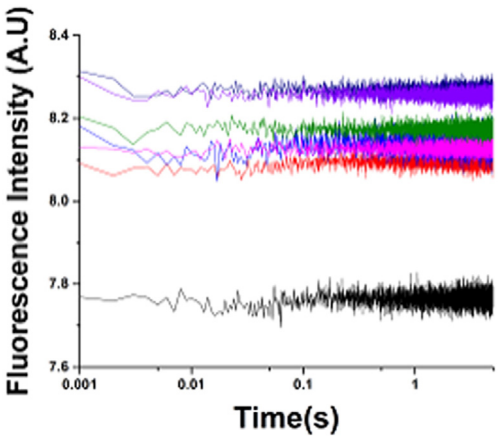

Fig. 5. Stopped-flow fluorescence traces of the A1095AP U-turn hairpin construct. Black trace is the control addition of buffer only. Adding $MgCl_2$ to 3, 5, 8, 20, 80, and 100 mM results in an immediate increase in fluorescence intensity but no subsequent transitions. Experiments with other hairpins showed similar, rapid intensity changes. [RNA] = 100 nM in 100 mM KCl and 10 mM sodium cacodylate (pH 6.5) at 20 °C.

Please cite this article as: R. Welty, K. B. Hall, Nucleobases Undergo Dynamic Rearrangements during RNA Tertiary Folding, J. Mol. Biol. (2016), http://dx.doi.org/10.1016/j.jmb.2016.09.015

Discussion

Direct observation of nucleobases in the GAC reveals their conformational excursions during the folding process, with conformational transitions on time scales from microseconds to tens of seconds. Some of these transitions are local, such as those in the loops, but others report on global rearrangements of the RNA as it forms a tertiary structure. This is the first comprehensive study of the nucleobases themselves during RNA tertiary folding.

Defining the structures of the starting and ending states

In their review of three-way junctions, Lescoute and Westhof [45] included the GAC. The goal of their analysis was to formulate rules that would allow the prediction of RNA tertiary folds. Their conclusion, based on a compendium of three-way junctions, was that the diversity of interactions essentially precludes prediction. However, joint consideration of RNA sequence and structural homology offered some suggestions of possible topologies. For example, if the secondary structure of an RNA includes a loop sequence that is known to form a GNRA tetraloop, then it can be modeled with that structure. Since GNRA tetraloops dock with a receptor, the RNA can then be examined to identify receptors. More generally, predicting the tertiary fold of an RNA requires the knowledge of the starting structure in order to identify discrete elements that could interact.

The secondary structure of the U1061A GAC [1] defines our starting state in the folding pathway. Hydroxyl radical footprinting of the GAC secondary structure showed that the hairpin loops and the three-way junction are unstructured in the absence of Mg^{2+} [12]. The 4-nt U-turn that caps the 3′ hairpin was previously investigated by solution NMR [46,47]. We have extended those studies to compare the loop properties as a function of temperature and Mg^{2+} (SF 5), and we conclude that the U-turn structure is present in the unfolded RNA and is stabilized by Mg^{2+}. In contrast, nucleotides in the T+loop appear to be unstructured based on previous NMR data [48] and hydroxyl radical probing. In summary, we define the starting structure of the U1061A GAC as two hairpins, one with an unstructured loop and one with a U-turn conformation, joined to a terminal stem by a disordered three-way junction.

We posit that the ending state is similar to the tertiary structure found in the cocrystals. Structure probing of the GAC under folded conditions (20 mM K-Mops and 5 mM $MgCl_2$) in the presence and absence of the L11 protein gave nearly identical patterns, supporting this assumption [12]. Our NMR experiments with selectively ^{15}N-labeled GAC are in agreement, as we observed the formation of four long-range hydrogen bonds from specific G and U imino protons (^{15}N–^{1}H) only when Mg^{2+} is present [36], as predicted from the cocrystal structures.

Temporal events in the folding pathway

Between these starting and ending states, we propose that the folding pathway contains four resolvable intermediate conformational states of the GAC. Folding is hierarchical, but the populations of each state are not uniquely present as illustrated. There is a dynamic equilibrium of conformational states, particularly in the final tertiary structure (3°) that contains I_3 and I_4.

$$2^\circ + Mg^{2+} \underset{k_{-1}}{\overset{k_1}{\leftrightarrow}} I_1 \underset{k_{-2}}{\overset{k_2}{\leftrightarrow}} I_2 + Mg^{2+} \underset{k_{-3}}{\overset{k_3}{\leftrightarrow}} I_3 \underset{k_{-4}}{\overset{k_4}{\leftrightarrow}} I_4 \underset{k_{-5}}{\overset{k_5}{\leftrightarrow}} 3^\circ$$

2° is the starting conformational state. I_1 corresponds to the initial loop relaxation and I_2 corresponds to the putative partial global collapse. I_3 represents the first state after a second Mg^{2+} interaction, I_4 represents the formation of the tertiary contacts, and 3° represents the last populated state, which exists in a dynamic equilibrium.

The first transitions contain information on both local conformations and global folding events, which are represented by I_1 and I_2 in our pathway scheme. The intermediate I_1 can be explained as a conformational change due to the relaxation of the single-stranded regions. We propose that the second intermediate I_2 is the result of a partial electrostatic collapse of the GAC. Previous Mg^{2+}-induced RNA folding experiments by Das *et al.* [20] have shown that partial RNA compaction is identifiable by time-resolved SAXS within milliseconds of interacting with Mg^{2+}.

The first observable transition (τ_1 = ~30 ms) occurs in every labeled element of the GAC. The relaxation time increases as Mg^{2+} concentration is increased until approximately 20 mM $MgCl_2$, where it reaches a plateau. This phenomenon, an increase in relaxation time as a function of increasing ligand concentration, is only observed if there is a rate-limiting kinetic step preceding a binding event [38]. By coupling this observation with the identification of I_1 and I_2, we conclude that I_2 accepts an Mg^{2+} ion. Therefore, we assign the third intermediate, I_3, to the conformation of the GAC when Mg^{2+} is chelated.

The presence of two longer relaxation times (τ_2, τ_3) is evidence that there are three states [37] that are populated after the Mg^{2+} chelation event. We choose to represent the final three states in our proposed pathway as sequential isomerizations. Each relaxation time does not solely represent single isomerization steps but rather represents multiple kinetic steps. As such, the three latter states are probably all present after chelation and exist in a dynamic equilibrium.

Please cite this article as: R. Welty, K. B. Hall, Nucleobases Undergo Dynamic Rearrangements during RNA Tertiary Folding, J. Mol. Biol. (2016), http://dx.doi.org/10.1016/j.jmb.2016.09.015

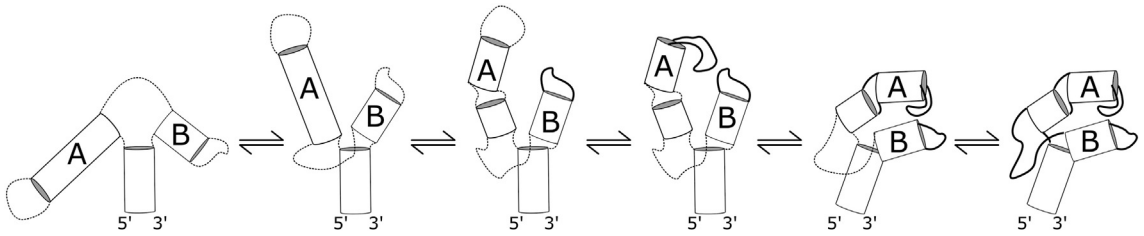

Fig. 6. Visualization of a possible folding scheme. The first structure is the starting secondary structure. The second is formed in <1.5 ms and illustrates electrostatic relaxation upon the addition of Mg^{2+} ions. The third structure is the counterion collapsed state. In the fourth structure, the T+loop structure is changed when specific Mg^{2+} ions associate, leading to a state where the second ion binding occurs when the hairpins interact. Finally, the last state is the tertiary structure.

The physical process of GAC folding

The progress curves provide some clues about the structural rearrangements of the GAC as it folds (Fig. 6 represents our model). We separate the traces into three time regimes: 1 to 100 ms, 100 ms to 1 s, and 1 to 100 s. In our folding scheme, I_1 and I_2 are formed prior to the first time interval, so the progress curves are reporting on the formation of I_3, I_4, and the final tertiary fold.

All sites experience conformational changes within the first 100 ms of folding. A1061AP in the internal bulge of the hairpin moves out of a stacked conformation. Its fluorescence intensity reaches a maximum at 100 ms at 20 °C, with an amplitude that is Mg^{2+}-dependent. If we assume that A1061AP is partially stacked in the internal bulge in its initial conformation, then the addition of Mg^{2+} results in a realignment of this bulge/stem in what could be a direct ion association or a result of a long-range interaction that distorts the bulge. The structure of this internal bulge with or without Mg^{2+} is not known, but NMR structures of an A:G mismatch juxtaposed to a U:U pair show distorted geometries of both pairs [49].

In the same time interval, nucleobases in the T+loop exhibit a variety of conformational changes. A1070AP begins to recover fluorescence intensity after its intensity loss during the initial rapid phase but does not reach a maximum value until about 3 s. A1067AP continues to lose fluorescence intensity after its initial, rapid Mg^{2+}-dependent loss. A1069AP fluorescence initially drops but is then constant until ~90 ms when it begins to decrease. The Mg^{2+} dependence of each T+loop nucleobase is consistent with a Mg^{2+}-dependent conformational change. We cannot determine from our data if the motions of the nucleobases are correlated or independent or if the T-loop conformational change is a cooperative transition.

In the cocrystal structures [2,3], A1061 is stacked with A1070, forming a long-range stacking interaction. If it forms in solution, without L11 protein, it is not stable, since the fluorescence intensity of A1070AP-GAC is too high to be consistent with a predominantly stacked state. Also, time-resolved anisotropy shows that A1061AP-GAC undergoes local motion on a nanosecond timescale (Supplementary Table 1). However, both sites are sensitive to Mg^{2+} ions and undergo a rearrangement of their environments during folding.

A1095AP fluorescence intensity decreases from 1 to 100 ms. The progress curves indicate that it undergoes a transient conformational change during GAC folding. This U-turn forms without Mg^{2+}, as do several others [50,51], so we could be seeing a contribution from the entire GAC to this local environment.

During the interval from 100 ms to 1 s, all 2AP sites exhibit large changes in fluorescence intensity. We assign these transitions to the global fold of the GAC as it approaches its tertiary structure, consistent with stopped-flow absorbance data. Several sites, A1061AP, A1070AP, and A1095AP, have large Mg^{2+}-dependent intensity changes, suggesting that ions are directly involved in their conformational transitions. Fluorescence intensities of other 2AP sites are much less dependent on the Mg^{2+} concentration. In our folding scheme, we consider I_4 to be the first intermediate to contain most tertiary contacts. Based on the progress curves, we conclude that I_4 and 3° are most likely to comprise the conformational ensemble after 1 s.

The time-courses from the A1089AP GAC are of particular interest since its major large transition is delayed, relative to the other sites. It was designed to report on the conformational transition of the three-way junction from unstructured to a triloop, but several explanations could account for this delayed response. It is possible that the triloop can only form after the other tertiary contacts have anchored the hairpins. Alternatively, A1089AP could be more sensitive to the formation of the conserved U1060–A1088 long-range hydrogen bond, which is formed late in the folding pathway. It is always possible that the A1089AP substitution could interfere with normal tertiary structure formation, perhaps transient misfolding/destabilization that leads to an increased relaxation time. Assuming that it does report on the conformational change of the junction, then we

Please cite this article as: R. Welty, K. B. Hall, Nucleobases Undergo Dynamic Rearrangements during RNA Tertiary Folding, J. Mol. Biol. (2016), http://dx.doi.org/10.1016/j.jmb.2016.09.015

would conclude that triloop formation is not stable in the absence of other tertiary contacts, and so, it forms last.

We hypothesize that the final 1- to 100-s interval represents conformational sampling by the GAC. The amplitude of this transition is small for all sites, suggesting that this state(s) is less populated and/or that its fluorescence signal is only subtlety different from the preceding conformation. Either alone or together, these conclusions suggest that the GAC is sampling iso-energetic conformations and exists not as a single conformation but in a dynamic equilibrium [52,53].

The T+loop

We consider this 9-nt loop to be at the heart of GAC folding. It must adopt a contorted structure to display four of its nucleotides for intramolecular interactions. It displays its phosphodiester backbone to create a pocket for ion chelation. Its extruded nucleobases make long-range base stacking interactions or base triples that anchor the three-way junction. We refer to it as a T+loop to distinguish it from typical T-loops [31,32].

tRNA T-loops

The first T-loop was observed in X-ray crystal structures of yeast $tRNA^{Phe}$ [54,55], where the 7-nt TψC loop [$T_{54}ψ_{55}CGA_{58}U_{59}C_{60}$] extruded $U_{59}C_{60}$ by the formation of a 5-nt loop closed by a T54–A58 reverse Hoogsteen pair. A striking feature of the $T_{54}ψ_{55}CGA_{58}$ loop structure was a sharp turn formed by $ψ_{55}CG$, and indeed, this portion of the TψC loop was identified as a U-turn structure (U-turn sequences are typically 5′UNR [33], where N is any nucleobase and R is a purine). The TψC loop is thus a loop within a loop, which is a structural characteristic of T-loops. Subsequent sequence searches for more T-loops found several [31], but more were identified by structural homology to the TψC loop [56] using existing crystal structures.

T-loops are typically involved in intramolecular or intermolecular RNA–RNA interactions, at times using their extruded bases and also the nucleotides within their U-turn. Their propensity for making intramolecular interactions makes them a common tertiary structure motif, and they are found in phylogenetically conserved regions of RNAs [56]. In yeast $tRNA^{Phe}$, nucleotides $ψ_{55}C_{56}$ make hydrogen bonds to nucleotides in the D-loop, effectively anchoring the characteristic tRNA L-shape. When Chan *et al.* [56] searched for T-loops in non-coding RNAs, they focused their analysis on the U-turn portion of the motif.

The T+loop

The GAC 1065–1073 loop is notable among T-loops for several reasons, which led us to designate it as a T+loop. First, it does not use nt1(U1065) and nt5 (A1069) to form a loop within a loop. Instead, it uses nt1 and nt9 (A1073) to form a Hoogsteen pair that closes the loop. It does form a U-turn-like structure with U1066A1067G1068A1069 (nt2–nt5), but then A1070, G1071, and C1072 are extruded and solvent-exposed. G1071 and C1072 make hydrogen-bonded base triples with the stem of hairpin B to anchor the tertiary structure. A1070 is stacked with U1061. This structure is observed in both cocrystals of GAC with L11 proteins, one with *E. coli* GAC (1hc8) [2] and the other with *Thermotoga maritima* GAC (1mms) [3]. The same GAC structure is found in the crystal structure of *E. coli* 70S ribosome with its bound L11 protein [6] (2.86 Å resolution).

The T+loop sequence differs in prokaryotes and eukaryotes, but it is conserved in yeast and humans: A1979UGGA1983AG1985UC1987 (using human ribosomal RNA numbering). Statistics of base conservation among all kingdoms shows significant diversity at very few sites (U:68%/A20%. U93%. A77%/G23%. G96%. A92%. A98%. G100%. C80%/U20%. A80%/C18%) [8]. In crystal structures of *Saccharomyces cerevisiae* [58] (pdb 3u5b, 3.0 Å resolution) ribosomes and in cryo-electron microscopy structures of human ribosomes [59] (pdb 3j3f, 5 Å resolution), the T+loop backbone structure is similar to that of prokaryotes (Fig. 7), and some base orientations vary.

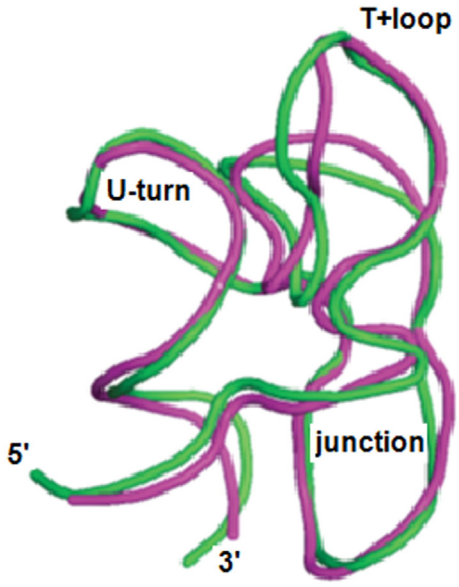

Fig. 7. Backbone trace of human [59] (pink) and *Thermus* [60] (green) GACs from ribosome crystal structures. Most of the variation is in the T+loop and the junction phosphodiester backbone. *Thermus* ribosome lacked L11 and human ribosome includes L12 (equivalent to L11) bound to the GAC.

Please cite this article as: R. Welty, K. B. Hall, Nucleobases Undergo Dynamic Rearrangements during RNA Tertiary Folding, J. Mol. Biol. (2016), http://dx.doi.org/10.1016/j.jmb.2016.09.015

Significantly, an NMR study of the yeast $tRNA^{Phe}$ TψC loop [61] failed to find any evidence of loop structure in the absence of Mg^{2+}. Those authors described the loop as seriously flexible. If the GAC T+loop is also unstructured in the absence of Mg^{2+}, then when does it adopt its T+ structure? Does the addition of Mg^{2+} cause a conformational change that allows it to dock with stemloop B? Or does it only adopt its T+ structure in the presence of stemloop B and Mg^{2+} via induced fit? This level of mechanistic detail is necessary to understand how the RNA uses this conserved loop to adopt its tertiary structure.

Properties of a canonical T-loop

The *Tetrahymena* group 1 intron P5c subdomain includes a 4- to 5-nt GNRA T-loop [62]. Formation of its canonical U-turn/extruded nucleobase structure is Mg^{2+}-dependent [63], and its conformational change triggers subsequent tertiary interactions of the P5c domain [19]. In kinetics experiments, its folding rate decreases with increasing Mg^{2+} concentration [64], which we suggest identifies the mechanism of its interaction with its ligand as a conformational selection [38]. An NMR investigation of P5c shows that its hairpin loop undergoes a conformational change with a rate of ~323 s^{-1} (3 ms) in 10 mM sodium phosphate (pH 6.4), which becomes faster in 1 mM $MgCl_2$ (964 s^{-1}; 1 ms) [65]. As an isolated hairpin, the native structure is seen as a low-abundance state, indicating that it requires tertiary contacts to stabilize its structure.

While T-loops are clearly important tertiary motifs, predicting their structures and identifying their interacting partners will be a challenge. Perhaps their sequence and conformational space are too large to allow such prediction. If loops are disordered in their starting state, then what are the rules that govern their final topology? More examples need to be studied to understand how their nucleotides sample their environments and find their targets.

Materials and Methods

RNA samples

Unlabeled GAC RNA was transcribed *in vitro* with T7 RNA polymerase via run-off transcription from plasmid DNA. The 2AP 60-mer constructs were chemically synthesized [30] by Agilent laboratories. The hairpin 2AP constructs were purchased from Integrated DNA technologies. All RNAs were dialyzed against 0.5 M EDTA and then into 100 mM KCl and 10 mM sodium cacodylate (pH 6.5). We used the Leipply and Draper laboratory protocol [12] to fold the full GAC RNAs into their proper secondary structure by heating to 65 °C for 30 min in 100 mM KCl and 10 mM sodium cacodylate (pH 6.5) and then by cooling at room temperature for 15 min. We folded the hairpin RNAs by heating to 95 °C for 5 min in 100 mM KCl and 10 mM sodium cacodylate (pH 6.5) and by immediately cooling on ice.

Absorbance thermal denaturation

Thermal denaturation was monitored in absorbance experiments on a Gilford 260 fitted with a Gilford thermoprogrammer 2527. RNA and $MgCl_2$ concentrations were 2 μM and 3 mM, respectively. Temperature was ramped at 0.5 °C per minute from 6 to 90 °C, while absorbance was recorded at 260 and 280 nm.

Fluorescence melt/titration

Fluorescence thermal denaturation and titrations experiments were performed on an Photon Technology International spectrofluorometer fitted with Peltier-controlled 4-cuvette turret. Samples were excited at 308 nm, and fluorescence emission was measured at 368 nm. Data points are the average of five consecutive measurements with an integration time of 1 s. For thermal denaturation experiments, the RNA concentration was 2 μM and the $MgCl_2$ concentration was 3 mM in 100 mM KCl and 10 mM sodium cacodylate (pH 6.5). Temperature was ramped at 1 °C per minute.

For fluorescence titrations, the RNA concentration was 1 μM and the temperature was controlled to 20 °C. The error bars were calculated using the standard deviation of the fluorescence measurements and an assumed 5% uncertainty in pipette volume. Titration data curves were not fit to a thermodynamic binding model, as it is impossible to distinguish between specific binding and nonspecific Mg^{2+} interaction.

Fluorescence lifetime/anisotropy

Time-correlated single photon counting and time-resolved anisotropy measurements were performed on a home-built instrument [66,67]. Lifetime and anisotropy data were fit using Fluofit Pro 4.4 (Picoquant) to a sum of exponentials. For lifetime analysis, $I(t)$ is the fluorescence intensity as a function of time t, τ_i is the lifetime of the ith component, and A_i is the pre-exponential factor of the ith component. For anisotropy analysis, R_0 is the initial steady-state anisotropy, βi is the amplitude of the ith component, and φ_i is the depolarization decay time. Anisotropy data for a given set of conditions (i.e., presence or absence of Mg^{2+}) were simultaneously fit, where φ_1 was constant.

$$I(t) = \sum_t A_t e^{\frac{-t}{\tau_i}} \qquad \text{S. EQ1}$$

$$r(t) = R_0 + \sum_i \beta_i e^{\frac{-t}{\varphi_i}} \qquad \text{S. EQ2}$$

Stopped-flow experiments

Stopped-flow experiments were performed on an Applied Photophysics SX-20 stopped-flow spectrometer. Time-courses were monitored over 105 s, with 5000 points taken uniformly in the first 5 s, and 10,000 uniformly spaced points were taken over the next 100 s. All measurements

Please cite this article as: R. Welty, K. B. Hall, Nucleobases Undergo Dynamic Rearrangements during RNA Tertiary Folding, J. Mol. Biol. (2016), http://dx.doi.org/10.1016/j.jmb.2016.09.015

were taken at 20 ± 0.1 °C. The time-courses are an average of ≥5 independent time-courses. Progress curves for A1061AP, A1067AP, A1070AP, and A1095AP were simultaneously fit to Eq. (1), and all relaxation times were globally shared; the A1089AP data were fit separately. There was no significant difference between X^2 and residuals generated from the global fits, and the individual time-courses fit independently. Curve fitting was done using the Origin software package.

Acknowledgments

We thank Michael Rau for many discussions and NMR experiments. We thank Professor Roberto Galletto for the use of his stopped-flow spectrometer. 2AP-GAC RNAs were received from Agilent labs, and we especially thank Dr. Laura-Kay Bruhn and Dr. Doug Dellinger for making these experiments possible. This research was supported in part by NIH NIGMS to K.B.H.

Appendix A. Supplementary Data

Supplementary data to this article can be found online at http://dx.doi.org/10.1016/j.jmb.2016.09.015.

Received 5 July 2016;
Received in revised form 31 August 2016;
Accepted 15 September 2016
Available online xxxx

Keywords:
GTPase center RNA;
2-aminopurine fluorescence;
RNA folding kinetics;
stopped-flow fluorescence

Abbreviations used:
GAC, GTPase center; 2AP, 2-aminopurine; SAXS, small angle X-ray scattering; rRNA, ribosomal RNA.

References

[1] A.S. Petrov, C.R. Bernier, B. Gulen, C.C. Waterbury, E. Hershkovits, C. Hsiao, S.C. Harvey, N.V. Hud, G.E. Fox, R.M. Wartell, L.D. Williams, Secondary structures of rRNAs from all three domains of life, PLoS One 9 (2014), e88222.

[2] G.L. Conn, A.G. Gittis, E.E. Lattman, V.K. Misra, D.E. Draper, A compact RNA tertiary structure contains a buried backbone–K^+ complex, J. Mol. Biol. 318 (2002) 963–973.

[3] B.T. Wimberly, R. Guymon, J.P. McCutcheon, S.W. White, V. Ramakrishnan, A detailed view of a ribosomal active site: the structure of the L11–RNA complex, Cell 97 (1999) 491–502.

[4] Y.-G. Gao, M. Selmer, C.M. Dunham, A. Weixlbaumer, A.C. Kelley, V. Ramakrishnan, The structure of the ribosome with elongation factor G trapped in the post-translocational state, Science 326 (2009) 694–699.

[5] E. Svidritskiy, A.F. Brilot, C.S. Koh, N. Grigorieff, A.A. Korostelev, Structures of yeast 80S ribosome–tRNA complexes in the rotated and nonrotated conformations, Structure 22 (2014) 1210–1218.

[6] D.S. Tourigny, I.S. Fernández, A.C. Kelley, V. Ramakrishnan, Elongation factor G bound to the ribosome in an intermediate state of translocation, Science 340 (2013) 1,235,490.

[7] M. Lu, D.E. Draper, Bases defining an ammonium and magnesium ion-dependent tertiary structure within the large subunit ribosomal RNA, J. Mol. Biol. 244 (1994) 572–585.

[8] C.R. Bernier, A.S. Petrov, C.C. Waterbury, J. Jett, F. Li, L.E. Freil, X. Xiong, L. Wang, B.L.R. Migliozzi, E. Hershkovits, Y. Xue, C. Hsiao, J.C. Bowman, S.C. Harvey, M.A. Grover, Z.J. Wartell, L.D. Williams, RiboVision suite for visualization and analysis of ribosomes, Faraday Discuss. 169 (2014) 195–207.

[9] C. Maeder, G.L. Conn, D.E. Draper, Optimization of a ribosomal structural domain by natural selection, Biochemistry 45 (2006) 6635–6643.

[10] D. Grilley, V. Misra, G. Caliskan, D.E. Draper, Importance of partially unfolded conformations for $Mg(^{2+})$-induced folding of RNA tertiary structure: structural models and free energies of Mg^{2+} interactions, Biochemistry 46 (2007) 10,266–10,278.

[11] R. Shiman, D.E. Draper, Stabilization of RNA tertiary structure by monovalent cations, J. Mol. Biol. 302 (2000) 79–91.

[12] D. Leipply, D.E. Draper, Evidence for a thermodynamically distinct Mg^{2+} ion associated with formation of an RNA tertiary structure, J. Am. Chem. Soc. 133 (2011) 13,397–13,405.

[13] J.R. Williamson, Induced fit in RNA–protein recognition, Nat. Struct. Biol. 7 (2000) 834–837.

[14] Y. Wan, H. Suh, R. Russell, D. Herschlag, Multiple unfolding events during native folding of the *Tetrahymena* group I ribozyme, J. Mol. Biol. 400 (2010) 1067–1077.

[15] S.V. Solomatin, M. Greenfeld, S. Chu, D. Herschlag, Multiple native states reveal persistent ruggedness of an RNA folding landscape, Nature 463 (2010) 681–684.

[16] D. Mitchell, R. Russell, Folding pathways of the *Tetrahymena* ribozyme, J. Mol. Biol. 426 (2014) 2300–2312.

[17] D. Mitchell, I. Jarmoskaite, N. Seval, S. Seifert, R. Russell, The long-range P3 helix of the *Tetrahymena* ribozyme is disrupted during folding between the native and misfolded conformations, J. Mol. Biol. 425 (2013) 2670–2686.

[18] I. Shcherbakova, M. Brenowitz, Perturbation of the hierarchical folding of a large RNA by the destabilization of its scaffold's tertiary structure, J. Mol. Biol. 354 (2005) 483–496.

[19] A. Laederach, I. Shcherbakova, M.P. Liang, M. Brenowitz, R.B. Altman, Local kinetic measures of macromolecular structure reveal partitioning among multiple parallel pathways from the earliest steps in the folding of a large RNA molecule, J. Mol. Biol. 358 (2006) 1179–1190.

[20] R. Das, L.W. Kwok, I.S. Millett, Y. Bai, T.T. Mills, J. Jacob, G.S. Maskel, S. Seifert, S.G.J. Mochrie, P. Thiyagarajan, S. Doniach, L. Pollack, D. Herschlag, The fastest global events in RNA folding: electrostatic relaxation and tertiary collapse of the *Tetrahymena* ribozyme, J. Mol. Biol. 332 (2003) 311–319.

[21] S. Chauhan, R. Behrouzi, P. Rangan, S.A. Woodson, Structural rearrangements linked to global folding pathways

of the *Azoarcus* group I ribozyme, J. Mol. Biol. 386 (2009) 1167–1178.
[22] S. Moghaddam, G. Caliskan, S. Chauhan, C. Hyeon, R.M. Briber, D. Thirumalai, S.A. Woodson, Metal ion dependence of cooperative collapse transitions in RNA, J. Mol. Biol. 393 (2009) 753–764.
[23] R. Behrouzi, J.H. Roh, D. Kilburn, R.M. Briber, S.A. Woodson, Cooperative tertiary interaction network guides RNA folding, Cell 149 (2012) 348–357.
[24] K.R. Gleitsman, D.H. Herschlag, A kinetic and thermodynamic framework for the *Azoarcus* group I ribozyme reaction, RNA 20 (2014) 1732–1746.
[25] I. Shcherbakova, S. Gupta, M.R. Chance, M. Brenowitz, Monovalent ion-mediated folding of the *Tetrahymena thermophila* ribozyme, J. Mol. Biol. 342 (2004) 1431–1442.
[26] B. Sclavi, M. Sullivan, M.R. Chance, M. Brenowitz, S.A. Woodson, RNA folding at millisecond intervals by synchrotron hydroxyl radical footprinting, Science 279 (1998) 1940–1943.
[27] Y. Wan, R. Russell, Enhanced specificity against misfolding in a thermostable mutant of the *Tetrahymena* ribozyme, Biochemistry 50 (2011) 864–874.
[28] S. Sinan, X. Yuan, R. Russell, The *Azoarcus* group I intron ribozyme misfolds and is accelerated for refolding by ATP-dependent RNA chaperone proteins, J. Biol. Chem. 286 (2011) 37,304–37,312.
[29] R. Russell, R. Das, H. Suh, K.J. Travers, A. Laederach, M.A. Engelhardt, D. Herschlag, The paradoxical behavior of a highly structured misfolded intermediate in RNA folding, J. Mol. Biol. 363 (2006) 531–544.
[30] D.J. Dellinger, Z. Timár, J. Myerson, A.B. Sierzchala, J. Turner, F. Ferreira, Z. Kupihár, G. Dellinger, K.W. Hill, J.A. Powell, J.R. Sampson, M.H. Caruthers, Streamlined process for the chemical synthesis of RNA using 2′-*O*-thionocarbamate-protected nucleoside phosphoramidites in the solid phase, J. Am. Chem. Soc. 133 (2011) 11,540–11,556.
[31] U. Nagaswamy, G.E. Fox, Frequent occurrence of the T-loop RNA folding motif in ribosomal RNAs, RNA 8 (2002) 1112–1119.
[32] A.S. Krasilnikov, A. Mondragón, On the occurrence of the T-loop RNA folding motif in large RNA molecules, RNA 9 (2003) 640–643.
[33] R.R. Gutell, J.J. Cannone, D. Konings, D. Gautheret, Predicting U-turns in ribosomal RNA with comparative sequence analysis, J. Mol. Biol. 300 (2000) 791–803.
[34] J.R. Lakowicz, Principles of Fluorescence Spectroscopy, 3rd edit. Springer, NY, 2006.
[35] J.M. Jean, K.B. Hall, 2-aminopurine fluorescence quenching and lifetimes: role of base stacking, Proc. Natl. Acad. Sci. U. S. A. 98 (2001) 37–41.
[36] M.J. Rau, R. Welty, W. Tom Stump, K.B. Hall, Formation of tertiary interactions during rRNA GTPase center folding, J. Mol. Biol. 427 (2015) 2799–2815.
[37] M. Starzak, Mathematical Methods in Chemistry and Physics, Plenum Press, NY, 1989.
[38] A.D. Vogt, E. Di Cera, Conformational selection or induced fit? A critical appraisal of the kinetic mechanism, Biochemistry 51 (2012) 5894–5902.
[39] K. Takamoto, R. Das, Q. He, S. Doniach, M. Brenowitz, D. Herschlag, M.R. Chance, Principles of RNA compaction: insights from the equilibrium folding pathway of the P4–P6 RNA domain in monovalent cations, J. Mol. Biol. 343 (2004) 1195–1206.
[40] R. Russell, I.S. Millett, M.W. Tate, L.W. Kwok, B. Nakatani, S.M. Gruner, S.G.J. Mochrie, V. Pande, S. Doniach, D. Herschlag, L. Pollack, Rapid compaction during RNA folding, Proc. Natl. Acad. Sci. U. S. A. 99 (2002) 4266–4271.
[41] S.A. Pabit, J.L. Sutton, H. Chen, L. Pollack, Role of ion valence in the submillisecond collapse and folding of a small RNA domain, Biochemistry 52 (2013) 1539–1546.
[42] J.H. Roh, L. Guo, J.D. Kilburn, R.M. Briber, T. Irving, S.A. Woodson, Multistage collapse of a bacterial ribozyme observed by time-resolved small-angle X-ray scattering, J. Am. Chem. Soc. 132 (2010) 10,148–10,154.
[43] D. Labuda, D. Poerschke, Magnesium ion inner sphere complex in the anticodon loop of tRNAPhe, Biochemistry 21 (1982) 49–53.
[44] H. Ma, D.J. Proctor, E. Kierzek, R. Kierzek, P.C. Bevilacqua, M. Gruebele, Exploring the energy landscape of a small RNA hairpin, J. Am. Chem. Soc. 128 (2006) 1523–1530.
[45] A. Lescoute, E. Westhof, Topology of three-way junctions in folded RNAs, RNA 12 (2006) 83–93.
[46] M.A. Fountain, M.J. Serra, T.R. Krugh, D.H. Turner, Structural features of a six-nucleotide RNA hairpin loop found in ribosomal RNA, Biochemistry 35 (1996) 6539–6548.
[47] S. Huang, Y.X. Wang, D.E. Draper, Structure of a hexanucleotide RNA hairpin loop conserved in ribosomal RNAs, J. Mol. Biol. 258 (1996) 308–321.
[48] Y.X. Wang, S. Huang, D.E. Draper, Structure of a U.U pair within a conserved ribosomal RNA hairpin, Nucleic Acids Res. 24 (1996) 2666–2672.
[49] N. Shankar, T. Xia, S.D. Kennedy, T.R. Krugh, D.H. Mathews, D.H. Turner, NMR reveals the absence of hydrogen bonding in adjacent UU and AG mismatches in an isolated internal loop from ribosomal RNA, Biochemistry 46 (2007) 12,665–12,678.
[50] S.C. Stallings, P.B. Moore, The structure of an essential splicing element: stem loop IIa from yeast U2 snRNA, Structure 5 (1997) 1173–1185.
[51] S.R. Gottstein-Schmidtke, E. Duchardt-Ferner, F. Groher, J.E. Weigand, D. Gottstein, B. Suess, J. Wöhnert, Building a stable RNA U-turn with a protonated cytidine, RNA 20 (2014) 1163–1172.
[52] S. Hohng, T.J. Wilson, E. Tan, R.M. Clegg, D.M.J. Lilley, T. Ha, Conformational flexibility of four-way junctions in RNA, J. Mol. Biol. 336 (2004) 69–79.
[53] S.E. McDowell, J.M. Jun, N.G. Walter, Long-range tertiary interactions in single hammerhead ribozymes bias motional sampling toward catalytically active conformations, RNA 16 (2010) 2414–2426.
[54] G.J. Quigley, A. Rich, Structural domains of transfer RNA molecules, Science 194 (1976) 796–806.
[55] H. Shi, P.B. Moore, The crystal structure of yeast phenylalanine tRNA at 1.93 A resolution: a classic structure revisited, RNA 6 (2000) 1091–1105.
[56] C.W. Chan, B. Chetnani, A. Mondragón, Structure and function of the T-loop structural motif in noncoding RNAs. Wiley Interdiscip Rev RNA 4 (n.d.) 507–522.
[58] A. Ben-Shem, N. Garreau de Loubresse, S. Melnikov, L. Jenner, G. Yusupova, M. Yusupov, The structure of the eukaryotic ribosome at 3.0 Å resolution, Science 334 (2011) 1524–1529.
[59] A.M. Anger, J.-P. Armache, O. Berninghausen, M. Habeck, M. Subklewe, D.N. Wilson, R. Beckmann, Structures of the human and *Drosophila* 80S ribosome, Nature 497 (2013) 80–85.
[60] R.M. Voorhees, T.M. Schmeing, A.C. Kelley, V. Ramakrishnan, The mechanism for activation of GTP hydrolysis on the ribosome, Science 330 (2010) 835–838.

Please cite this article as: R. Welty, K. B. Hall, Nucleobases Undergo Dynamic Rearrangements during RNA Tertiary Folding, J. Mol. Biol. (2016), http://dx.doi.org/10.1016/j.jmb.2016.09.015

[61] L.J. Yao, T.L. James, J.T. Kealey, D.V. Santi, U. Schmitz, The dynamic NMR structure of the T psi C-loop: implications for the specificity of tRNA methylation, J. Biomol. NMR 9 (1997) 229–244.
[62] M. Wu, I. Tinoco, RNA folding causes secondary structure rearrangement, Proc. Natl. Acad. Sci. 95 (1998) 11,555–11,560.
[63] J.H. Cate, R.L. Hanna, J.A. Doudna, A magnesium ion core at the heart of a ribozyme domain, Nat. Struct. Biol. 4 (1997) 553–558.
[64] E. Koculi, S.S. Cho, R. Desai, D. Thirumalai, S.A. Woodson, Folding path of P5abc RNA involves direct coupling of secondary and tertiary structures, Nucleic Acids Res. 40 (2012) 8011–8020.
[65] Y. Xue, B. Gracia, D. Herschlag, R. Russell, H.M. Al-Hashimi, Visualizing the formation of an RNA folding intermediate through a fast highly modular secondary structure switch, Nat. Commun. 7 (2016) (ncomms11768).
[66] J.M. Jean, K.B. Hall, 2-aminopurine electronic structure and fluorescence properties in DNA, Biochemistry 41 (2002) 13,152–13,161.
[67] J.M. Jean, K.B. Hall, Stacking-unstacking dynamics of oligodeoxynucleotide trimers, Biochemistry 43 (2004) 10,277–10,284.

Please cite this article as: R. Welty, K. B. Hall, Nucleobases Undergo Dynamic Rearrangements during RNA Tertiary Folding, J. Mol. Biol. (2016), http://dx.doi.org/10.1016/j.jmb.2016.09.015